Acta Crystallographica Section D
Biological Crystallography
ISSN 1399-0047

Structure of the type VI secretion phospholipase effector Tle1 provides insight into its hydrolysis and membrane targeting

Haidai Hu,[a,b]‡ Heng Zhang,[b]‡ Zengqiang Gao,[b] Dongqi Wang,[c] Guangfeng Liu,[b] Jianhua Xu,[b] Ke Lan[a]* and Yuhui Dong[b]*

[a]Key Laboratory of Molecular Virology and Immunology, Institute Pasteur of Shanghai, Chinese Academy of Sciences, Shanghai 200025, People's Republic of China, [b]Beijing Synchrotron Radiation Facility, Institute of High Energy Physics, Chinese Academy of Sciences, Beijing 100049, People's Republic of China, and [c]Multidisciplinary Initiative Center, Institute of High Energy Physics, Chinese Academy of Sciences, Beijing 100049, People's Republic of China

‡ These authors made equal contributions to this work.

Correspondence e-mail: lanke@sibs.ac.cn, dongyuhui@ihep.ac.cn

Received 3 April 2014
Accepted 3 June 2014

PDB reference: Tle1, 4o5p

A diverse superfamily of phospholipases consisting of the type VI lipase effectors Tle1–Tle5 secreted by the bacterial type VI secretion system (T6SS) have recently been identified as antibacterial effectors that hydrolyze membrane phospholipids. These effectors show no significant homology to known lipases, and their mechanism of membrane targeting and hydrolysis of phospholipids remains unknown. Here, the crystal structure of Tle1 (~96.5 kDa) from *Pseudomonas aeruginosa* refined to 2.0 Å resolution is reported, representing the first structure of this superfamily. Its overall structure can be divided into two distinct parts, the phospholipase catalytic module and the putative membrane-anchoring module; this arrangement has not previously been observed in known lipase structures. The phospholipase catalytic module has a canonical α/β-hydrolase fold and mutation of any residue in the Ser-Asp-His catalytic triad abolishes its toxicity. The putative membrane-anchoring module adopts an open conformation composed of three amphipathic domains, and its partial folds are similar to those of several periplasmic or membrane proteins. A cell-toxicity assay revealed that the putative membrane-anchoring module is critical to Tle1 antibacterial activity. A molecular-dynamics (MD) simulation system in which the putative membrane-anchoring module embedded into a bilayer was stable over 50 ns. These structure–function studies provide insight into the hydrolysis and membrane-targeting process of the unique phospholipase Tle1.

1. Introduction

The type VI secretion system (T6SS), a novel multi-subunit needle-like apparatus, functions as both a virulence factor directly attacking host cells and as a mediator in bacterial interspecies competition (Jani & Cotter, 2010; Schwarz *et al.*, 2010). Gram-negative bacteria harbouring the T6SS inject effectors into the cytoplasm or periplasm of the recipient cells to kill them. Meanwhile, the cognate immunity proteins in the donor cells bind and neutralize the toxicities of the effectors to protect themselves (Hood *et al.*, 2010; Russell *et al.*, 2011). Our group and others have solved crystal structures of these effectors and their complexes with immunity proteins from several human pathogens such as *Pseudomonas aeruginosa*, *Salmonella typhimurium* and *Enterobacter cloacae*. Structure-based functional analysis revealed their diverse catalytic mechanisms and the mechanisms of inhibition by immunity proteins (Chou *et al.*, 2012; Ding *et al.*, 2012; Dong, Zhang *et al.*, 2013; Li *et al.*, 2013; Zhang *et al.*, 2013).

The membrane of Gram-negative bacteria is primarily composed of a phospholipid bilayer with many transmembrane proteins embedded into the membrane, and is a pivotal

component in the survival of these cells. It has many important physiological functions, such as serving as the location for transporting molecules into the cell and as a permeability barrier for most molecules. Very recently, a diverse superfamily of bacterial T6SS effectors, type VI lipase effectors 1–5 (Tle1–Tle5), with the role of mediating antagonistic bacterial interactions have been identified (Russell *et al.*, 2013). In this superfamily, Tle1, Tle2 and Tle5 possess phospholipase A_2, A_1 and D (PLA_2, PLA_1 and PLD) activities, respectively. These proteins can hydrolyze the membrane phospholipids of neighbouring cells with an increase in cellular permeability after being injected into their periplasmic space by the T6SS, whereas these antibacterial activities can be inhibited by their cognate immunity proteins type VI secretion lipase immunity 1, 2 and 5 (Tli1, Tli2 and Tli5), respectively (Russell *et al.*, 2013). Besides the Tle family members, VasX (VCA0020) and TseL (VC1418) from *Vibrio cholerae* have also been identified as T6SS-dependent antibacterial effectors with lipase activity (Dong, Ho *et al.*, 2013; Miyata *et al.*, 2011).

The Tle1–4 effector families possess the conserved G*X*S*X*G catalytic motif and Ser-Asp-His catalytic triad common to a diversity of esterase enzymes, including thioesterases, acetylesterases and assorted lipase and phospholipases (Russell *et al.*, 2013). However, these families lack significant homology to known lipase enzymes, suggesting that they may represent new members with distinct substrate-recognition and catalytic mechanisms in the lipase superfamily. Therefore, it is very important to discover how these effectors target membrane phospholipids and trigger the catalytic reactions. In this study, we determined the high-resolution crystal structure of Tle1 from *P. aeruginosa*, the first structural study of a T6SS phospholipase effector. Structural analysis revealed a conserved phospholipase catalytic module and a putative membrane-targeting module; this arrangement has not previously been observed in lipases. Further biochemical analysis showed that the putative membrane-targeting module is required for Tle1 toxicity. These studies provide structural insights into the catalytic mechanism of Tle1 targeting to membrane phospholipids and contribute to a better understanding of the antibacterial activities of the T6SS phospholipase effector family.

2. Methods

2.1. Cloning, protein expression and purification

The gene encoding full-length Tle1 was amplified from the *P. aeruginosa* PAO1 genomic DNA. The PCR product was digested and then cloned into the pET-28at(+) vector with an N-terminal His tag followed by a *Tobacco etch virus* (TEV) cleavage site. The expression plasmid was transformed into *Escherichia coli* strain BL21 (DE3) for expression. Site-directed mutagenesis of *tle1* was performed by a PCR-based technique according to the QuikChange site-directed mutagenesis strategy (Stratagene) following the manufacturer's instructions. The mutant genes were sequenced and found to contain only the desired mutations. Selenomethionine-derivatized (SeMet) Tle1 was produced and purified as described previously (Wei *et al.*, 2013).

Table 1
Data-collection and structure-refinement statistics.

Values in parentheses are for the highest resolution shell.

Data collection	
Wavelength (Å)	0.9792
Space group	*P*1
Unit-cell parameters (Å, °)	a = 61.603, b = 81.078, c = 92.145, α = 97.835, β = 89.958, γ = 90.010
Resolution (Å)	2.00 (2.03–2.00)
Unique reflections	109609 (5486)
Completeness (%)	92.3 (92.4)
Multiplicity	3.3 (3.1)
Mean $I/\sigma(I)$	24.6 (4.3)
Molecules in asymmetric unit	2
R_{merge} (%)	6.6 (21.2)
Structure refinement	
Resolution range (Å)	28.30–2.00
R_{work}/R_{free} (%)	22.8/26.9
Average B factor (Å^2)	
Main chain (molecule *A*/*B*)	24.91/24.74
Side chain (molecule *A*/*B*)	26.58/26.39
Waters	28.92
No. of residues (molecule *A*/*B*)	742/741
No. of atoms	
Protein (molecule *A*/*B*)	5753/5765
Waters	1025
Ramachandran plot (%)	
Most favoured	96.4
Allowed	3.6
R.m.s. deviations	
Bond lengths (Å)	0.008
Bond angles (°)	1.199

2.2. Crystallization, data collection, structure determination and refinement

Crystallization screens were performed with kits from Hampton Research and Qiagen using the sitting-drop vapour-diffusion method at 20 and 4°C. An SeMet Tle1 crystal was obtained in a solution consisting of 0.04 *M* citric acid, 0.06 *M* bis-tris propane pH 6.4, 20%(*w*/*v*) PEG 3350 after 6 d at 4°C. The crystal quality was optimized by adjusting the concentrations of the precipitant and the buffer. The best crystal was obtained in a solution consisting of 0.04 *M* citric acid, 0.1 *M* bis-tris propane pH 6.8, 17% PEG 3350 after 4 d at 4°C.

All data were collected on beamline 3W1A at Beijing Synchrotron Radiation Facility (BSRF) with a mounted MAR165 CCD detector. Before data collection, the crystals were soaked in reservoir solution supplemented with 20%(*v*/*v*) glycerol for a few seconds and then flash-cooled in liquid nitrogen. All data were processed using *HKL*-2000 (Otwinowski & Minor, 1997). The crystal structure of SeMet Tle1 was determined by the single-wavelength anomalous dispersion method. Se atoms were located using *SHELXD* (Sheldrick, 2010) and then used to calculate the initial phases in *SHELXE*. The phases from *SHELXE* were improved in *RESOLVE* (Terwilliger, 2000) and were then used for model building in *Buccaneer* (Cowtan, 2006). *Coot* (Emsley *et al.*, 2010) and *phenix.refine* (Adams *et al.*, 2010) were used for manual building and refinement, respectively. Refinement statistics and model parameters are given in Table 1. All

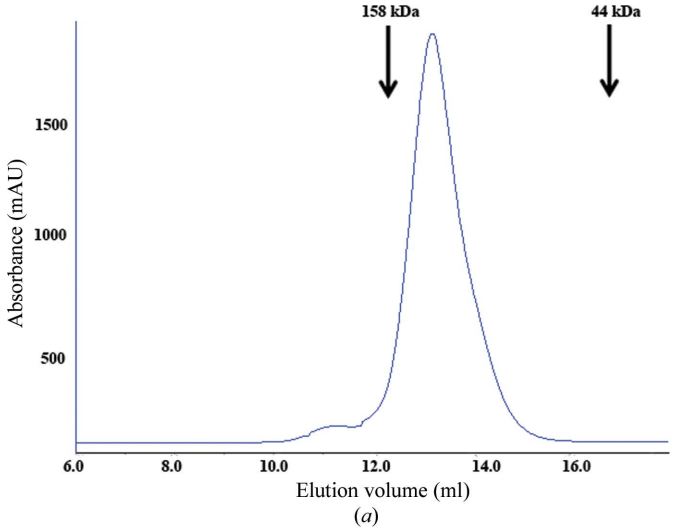

(*a*)

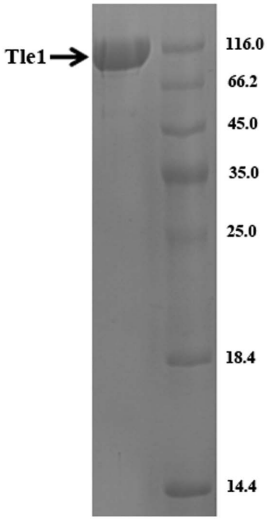

(*b*)

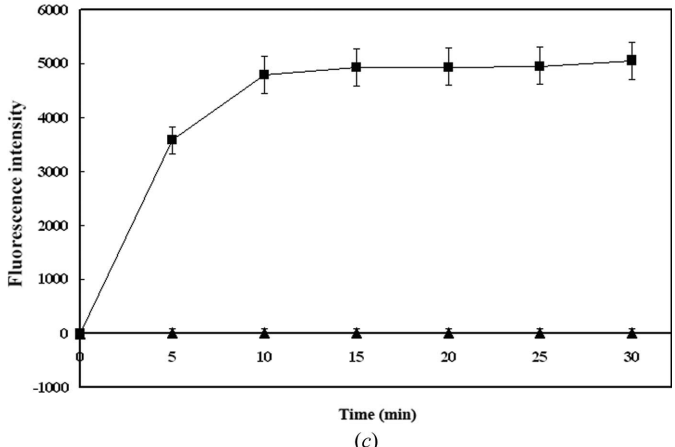

(*c*)

Figure 1
Solution characteristics of Tle1. (*a*) Purified Tle1 eluted from a gel-filtration chromatogram (Superdex 200 10/300 GL) at 12.5 ml, corresponding to a molecular mass of ∼100 kDa. (*b*) SDS–PAGE analysis of purified Tle1 visualized by Coomassie Blue (left lane). The right lane contains molecular-weight marker (labelled in kDa). (*c*) Enzymatic activity assay of purified Tle1 (squares; 5 mg ml^{-1}) *in vitro* using the fluorogenic phospholipid substrate PED6. The background (triangles) contained all components except Tle1. Error bars represent standard deviations from three independent experiments.

structural figures were prepared with *PyMOL* (DeLano, 2002). Superpositions of the structures were performed in *Coot* using *Secondary-Structure Matching* (*SSM*; Krissinel & Henrick, 2004).

2.3. *In vitro* PLA_2 activity assays of recombinant Tle1

The activity of the recombinant Tle1 was assayed using the fluorogenic phospholipid substrate PED6 according to the manufacturer's directions (Invitrogen). The reaction system consisted of 50 µl recombinant Tle1 prepared in assay buffer (50 m*M* Tris–HCl, 100 m*M* NaCl, 1 m*M* $CaCl_2$ pH 8.9) with 50 µl of the liposomally incorporated substrate added per sample microplate well. The background fluorescence was measured from reactions containing all components except Tle1. Fluorescence intensity was determined using a Tecan Infinite M200 Pro instrument (Tecan Group Ltd, Männedorf, Switzerland) with a band width of 20 nm, an excitation wavelength of 488 nm and an emission wavelength of 530 nm.

2.4. Cell-toxicity assay

The wild type and mutants of Tle1 were subcloned into the pET-22b vector containing N-terminal *pelB* signal-peptide sequences. A single colony harbouring the expression plasmid was grown in LB medium at 37°C. After overnight culture, the cells were serially diluted in tenfold steps and plated onto LB agar supplemented with 50 mg ml^{-1} ampicillin and 0.05 or 0.1 m*M* IPTG. The plates were prepared for imaging and plate counts after an additional ∼20 h of growth at 37°C. Protein-expression levels were detected at 2 h after induction by Western blot analysis against the anti-His antibody (Abmart, Shanghai, People's Republic of China) and SDS–PAGE analysis of these protein expressions with Coomassie Blue staining was used as a control.

2.5. Molecular-dynamics simulation

Missing residues in Tle1 were added using *MODELLER* 9.12 (Eswar *et al.*, 2006). Since the newly added C-terminus is highly flexible and is far away from the interaction site between the protein and the bilayer, the 49 residues at the C-terminus were not considered when preparing the protein model bound to a bilayer membrane, *i.e.* the 833 residues at the N-terminal end were used in model building and simulations. The net charge that the protein carries is −15. The bilayer used here contains 680 1-palmitoyl-2-oleoyl-*sn*-glycero-3-phosphoethanolamine (POPE) molecules, with its normal aligned with the z axis, and the box size is (x, y, z) = (19.14, 9.49, 6.66). *GROMACS* 4.5.6 (Hess *et al.*, 2008) was employed to prepare the model systems and to carry out the simulations. During the simulations, the protein was represented by the GROMOS96 53A6 parameter set (Oostenbrink *et al.*, 2004) and the POPE bilayer by a hybrid parameter set with GROMOS atom types and OPLS atomic partial charges (Berger *et al.*, 1997). Water was treated using the SPC model (Berendsen *et al.*, 1984). After initial energy minimization, the protein was aligned and embedded in the membrane using the *InflateGRO* methodology (Schmidt & Kandt, 2012). After the

system had been solvated in water, during which the van der Waals radius of the C atom was increased to avoid nonphysical solvation of the hydrophobic pore of the bilayer and restored afterwards, 14 water molecules were replaced by Na^+ cations based on the estimated electrostatic potential to neutralize the negative charges on Tle1 in order to make the whole system physically meaningful.

The system was then subjected to equilibration at a constant temperature of 310 K and a constant pressure of 1 atm for 1 ns, during which the protein was constrained to avoid unreasonable motions. After equilibration, the constraints were removed and the simulations were extended for a further 1 ns. The coordinates and atomic velocities of the final snapshot were used as the starting point of the production run, which lasted for 50 ns.

The box sizes of the equilibrated system are (17.27, 8.56, 11.69) for the model, which contains 32 452 water molecules and 534 POPE molecules. During the simulations, the time step was 2 fs and all bonds were constrained with the *LINCS* algorithm (Hess *et al.*, 1997). The pressure was kept constant using a Parrinello–Rahman barostat (Parrinello & Rahman, 1981) with a coupling time of 2.0 ps and with x–y and z being scaled independently. A Nosé–Hoover thermostat (Nosé, 1984) was used to keep the temperature at 310 K with a coupling time of 0.5 ps. Long-range electrostatics were calculated by the particle mesh Ewald method (Darden *et al.*, 1993).

3. Results

3.1. Purification of recombinant Tle1 from *P. aeruginosa*

A large number of putative T6SS phospholipase effectors Tle1–Tle5 from various species were selected for overexpression and most of them showed strong hydrophobicity and instability during the purification and crystallization processes. Interestingly, the overexpressed effector Tle1 (PA3290) from *P. aeruginosa* composed of 882 residues (∼96.5 kDa) was found to display relatively good hydrophilicity and stability under our purification conditions (Fig. 1*a*). The recombinant Tle1 had an apparent molecular mass of ∼100 kDa as determined by analytical size-exclusion chromatography (Fig. 1*b*), indicating that it exists as a monomer in solution. We then used the highly sensitive fluorogenic phospholipid substrate PED6 to examine the *in vitro* PLA_2 activity of Tle1. The results showed that Tle1-mediated hydrolysis of PED6 occurred over the time course tested (Fig. 1*c*). This confirmed that the recombinant Tle1 possessed PLA_2 activity, consistent with that from *Burkholderia thailandensis* (Russell *et al.*, 2013).

3.2. Overall structure of Tle1

The crystal structure of Tle1 from *P. aeruginosa* was solved by the single-wavelength anomalous dispersion (SAD) method from synchrotron data using SeMet protein refined to 2.0 Å resolution (Table 1). The asymmetric unit contains two Tle1 molecules comprising 742 and 741 residues, with overall dimensions of ∼60 × 55 × 85 Å, and a total of 1025 water molecules. Several regions, such as Glu44–Pro58, Trp663–Glu674 and Glu814–Leu882, which may be flexible, could not be observed in the electron-density map and were not included in the current model. Few interactions could be observed between the two NCS-related monomers with minor conformational variability, and this is likely to be the result of crystal packing and to have no biological relevance. The monomeric status is consistent with that in solution (Fig. 1*a*).

The overall structure of Tle1 adopts a complex arrangement with the striking feature that it can be divided into two distinct structural parts, termed the phospholipase catalytic module (Asn3–Glu450) and the putative membrane-anchoring module (Leu451–Val813) (Figs. 2*a* and 2*b*; Supplementary Fig. S1[1]). The catalytic module, with a compact conformation, displayed a classical mixed α/β-hydrolase fold that functions as the D1 phospholipase domain. It consists of seven central parallel β-sheets ($\beta1\uparrow$–$\beta9\uparrow$–$\beta8\uparrow$–$\beta6\uparrow$–$\beta4\uparrow$–$\beta2\uparrow$–$\beta3\uparrow$) in addition to two small twisted β-sheets ($\beta5$ and $\beta7$), flanked by 13 α-helices (11 α-helices and two η-helices) on both sides (Fig. 2*c* and Supplementary Fig. S1). The putative membrane-anchoring module, with a remarkable open conformation, hangs over the phospholipase catalytic module (Fig. 2*b*) and can be divided into three independent domains: D2, D3 and D4 (Fig. 2*c*). D2 is composed of two long helices ($\alpha15$ and $\alpha16$) and one short helix ($\alpha17$), forming a three-helix bundle, while D3 is composed of three long helices ($\alpha13$, $\alpha18$ and $\alpha19$) and three short helices ($\alpha12$, $\alpha14$ and $\alpha20$), forming a six-helix bundle. D4 has an α/β mixed fold and a remarkable feature is a two-layer sandwich structure formed by strands $\beta10$, $\beta12$, $\beta13$ and $\beta14$. In the module, the average of the atomic B factors for the linkers connecting the three domains is substantially higher than for the other regions (data not shown), suggesting that these segments comprise flexible linkers that connect the functional modules.

A *DALI* search (http://ekhidna.biocenter.helsinki.fi/dali_server) for globally similar proteins revealed that Tle1 has notable structural homology with the superfamily including lipid hydrolases, ester hydrolases, thioester hydrolases, peptide hydrolases, epoxide hydrolases and dehalogenases (Supplementary Table S1). The closest homologue is the serine cinnamoyl esterase LJ0536 from *Lactobacillus johnsonii* (PDB entry 3s2z; Lai *et al.*, 2011), with a *DALI* Z-score of 10.9 and an r.m.s.d. of 3.1 Å for 251 C^α atoms. However, notable similarity can only be observed in the catalytic module and the sequence identity between the module and its homologues is only ∼10%. The structural arrangement of Tle1 has not previously been observed in the lipase superfamily and is remarkably different from known structures. This suggests that the Tle1 structure may be unique and may represent a new member of the lipase superfamily.

3.3. Structural characteristics of the catalytic module

Despite significant efforts in soaking or co-crystallizing Tle1 with phospholipids or associated analogues, we have been

[1] Supporting information has been deposited in the IUCr electronic archive (Reference: QH5009).

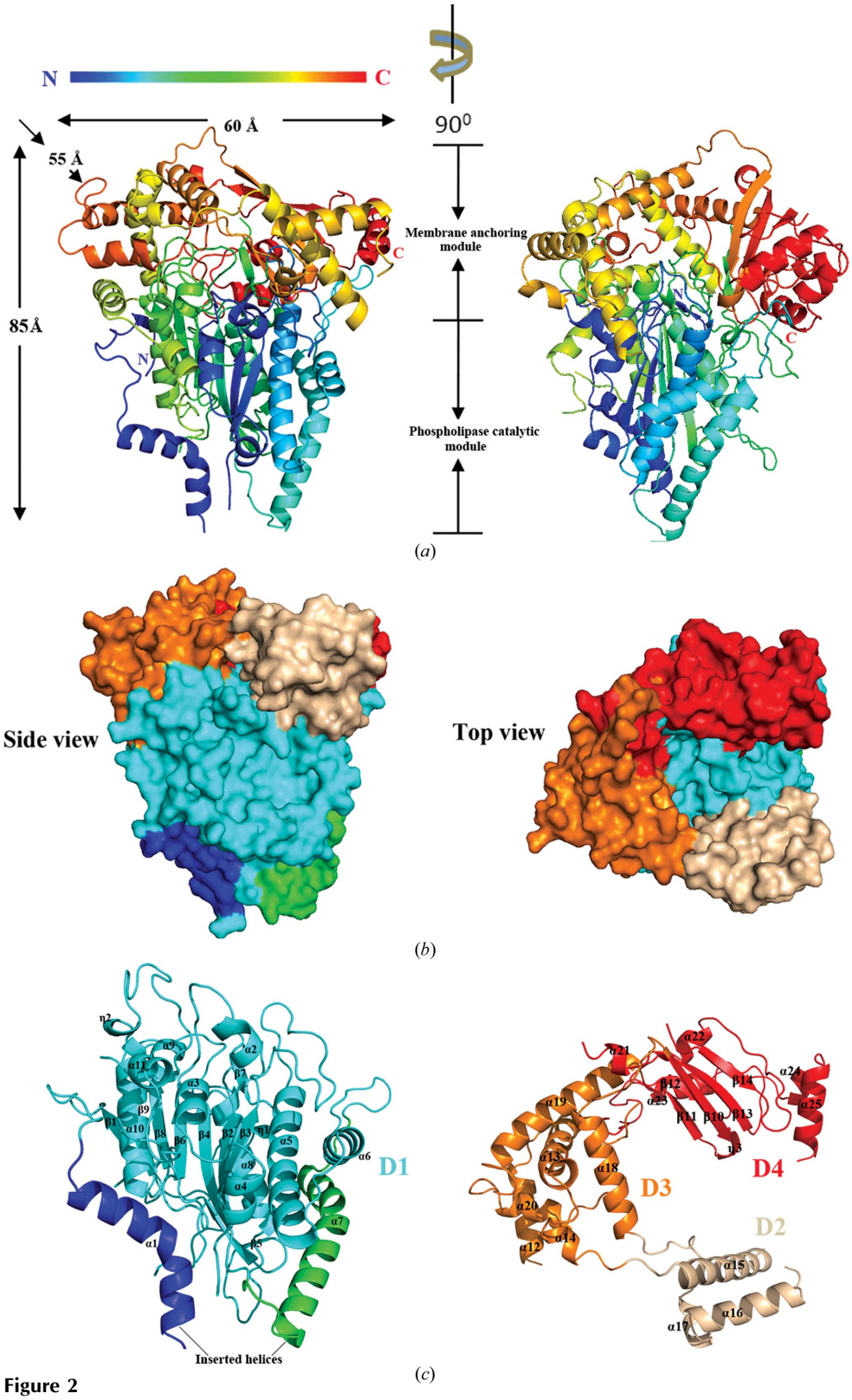

Figure 2
Structural characteristics of Tle1. (*a*) Overall view of the Tle1 structure colour-coded as a ramp from blue (N-terminus) through cyan, green, yellow and orange to red (C-terminus) and composed of two distinct parts: the phospholipase catalytic module and the membrane-anchoring module. (*b*) Surface representation showing a side view and a top view of the domain architecture of Tle1. The phospholipase catalytic module consists of the catalytic domain D1 (cyan) with two inserted helices α1 (blue) and α7 (green) located on the opposite side. The membrane-anchoring module with an open conformation is composed of domains D2 (wheat), D3 (orange) and D4 (red). (*c*) Cartoon representation showing the domain architecture of Tle1 with topology numbers labelled.

unable to collect usable crystallographic data for phospholipids bound to Tle1. Nonetheless, structural superimpositions of the module with ligand-bound homology structures uncover the highly conserved catalytic triad in the putative catalytic pocket (Fig. 3*a* and Supplementary Fig. S2*a*). Similar to the triacylglycerol lipase LipS (PDB entry 4fbl; Chow *et al.*, 2012) and the human membrane-associated monoglyceride lipase hMGL (PDB entry 3pe6; Schalk-Hihi *et al.*, 2011), the active site of Tle1 also adopts an extended and closed binding pocket with positive charge at the entrance to bind negatively charged phospholipid head groups (Supplementary Fig. S2*b*). The pocket contains the highly conserved catalytic triad Ser235–Asp279–His377 (Fig. 3*b*), with the catalytic serine residue located at the nucleophilic elbow formed between β4 and α8. Ser235 also takes part in the highly conserved serine esterase motif Gly231-Phe-Ser-Arg-Gly235 (Supplementary Fig. S1). The role of His377 is to deprotonate Ser235 so that Ser235 can perform a nucleophilic attack on the C atom of the carbonyl group of the substrate, while Asp279 stabilizes the protonated His377. The pocket, with a depth of ~15 Å, is formed not only by residues located in loops β2–α2, α2–α3, β4–α8, β6–β7, α9–η2 and helices α2 and α9, but also by extensions to the residues in both α12 and α20 from D3 (Fig. 3*c*). The cell-toxicity assay showed that wild-type Tle1 in the periplasmic space can severely inhibit the growth of *E. coli* (Fig. 3*d*), consistent with the toxicity of Tle1 from *B. thailandensis*, which can cause membrane destruction and increase the cellular permeability (Russell *et al.*, 2013). This suggests that Tle1 may function as a phospholipase with hydrolytic activity towards phospho-

lipids from bacterial membranes. Meanwhile, the mutation of any of the catalytic triad residues to alanine by site-directed mutagenesis abolished the toxicity (Fig. 3*d*), indicating that all of them are indispensable for catalytic activity and that the antibacterial effect of Tle1 is dependent on the catalytic domain. Consistently, the *in vitro* PLA_2 activity of the purified S235A and H377A mutants was ∼45 and ∼40% of that of wild-type Tle1, respectively (Supplementary Fig. S3). Our attempts to purify the D279A mutant yielded only insoluble products, suggesting that Asp279 is important for both the catalytic activity and the folding stability of Tle1.

The active-site pocket contains about two-thirds hydrophobic residues (*i.e.* Phe234, Phe278 and Phe342; Supplementary Fig. S1), which provide an amphipathic environment for substrate binding. Further analysis of the surface cavity of the catalytic pocket using the *Computed Atlas of Surface*

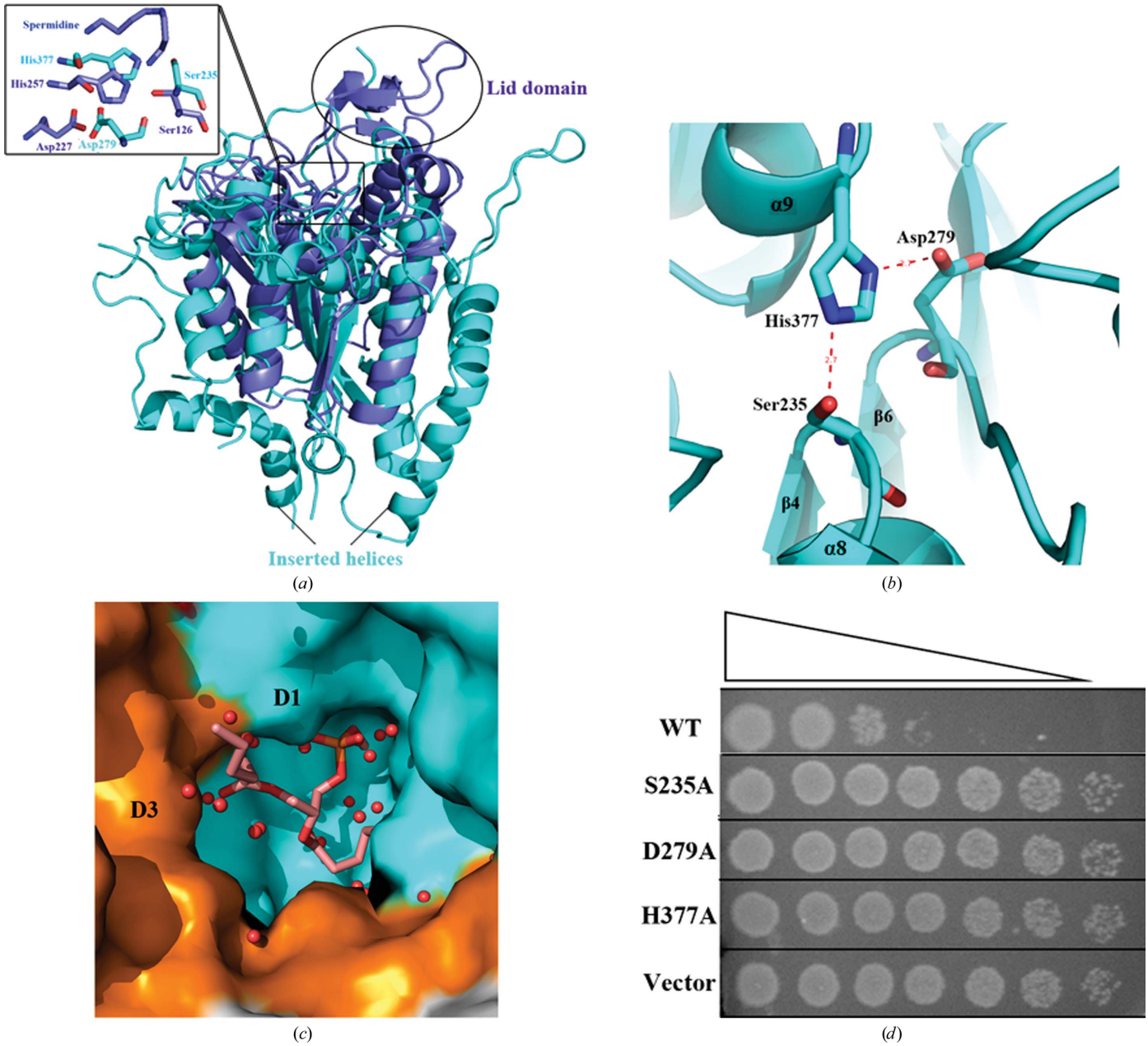

Figure 3
The catalytic site of Tle1. (*a*) Structural superposition of the phospholipase catalytic module (cyan) with LipS in complex with spermidine (purple; PDB entry 4fbl; Chow *et al.*, 2012). In the complex structure, the spermidine is remarkably close to the catalytic triad (Ser126, Asp187 and His257) and was thought to mimic substrate bound in the active site. Their similar catalytic sites are boxed and the remarkable inserted helices are labelled. The lid domain in LipS is indicated by an ellipse. (*b*) The catalytic triad residues Ser235–Asp279–His377 of Tle1 are properly placed to establish hydrogen bonds. (*c*) Docking model of a phosphatidylglycerol molecule (pink sticks; extracted from PDB entry 4bk2; Montersino *et al.*, 2013) into the closed conformation of the catalytic pocket composed of D1 (cyan) and part of D3 (orange). Waters found in the active site are depicted as red spheres. (*d*) Growth of *E. coli* in agar plates harbouring a vector expressing wild-type Tle1 and its mutants in the periplasm. The cells were prepared with serial tenfold dilutions from left to right.

Topography of proteins (*CASTp*) server (Dundas *et al.*, 2006) revealed that it has an area of 1188.5 Å^2 and a volume of 2066.3 Å^3. To determine whether the closed form of Tle1 can accommodate a substrate phospholipid molecule, we performed a docking study using *AutoDock* (Morris *et al.*, 1998). The docking model of the active site in the closed form shows that the pocket can accommodate a phospholipid molecule (Fig. 4*c*). The putative substrate phosphatidylglycerol is completely buried in the active site and displays the proper orientation for catalysis. The oxyanion hole is formed

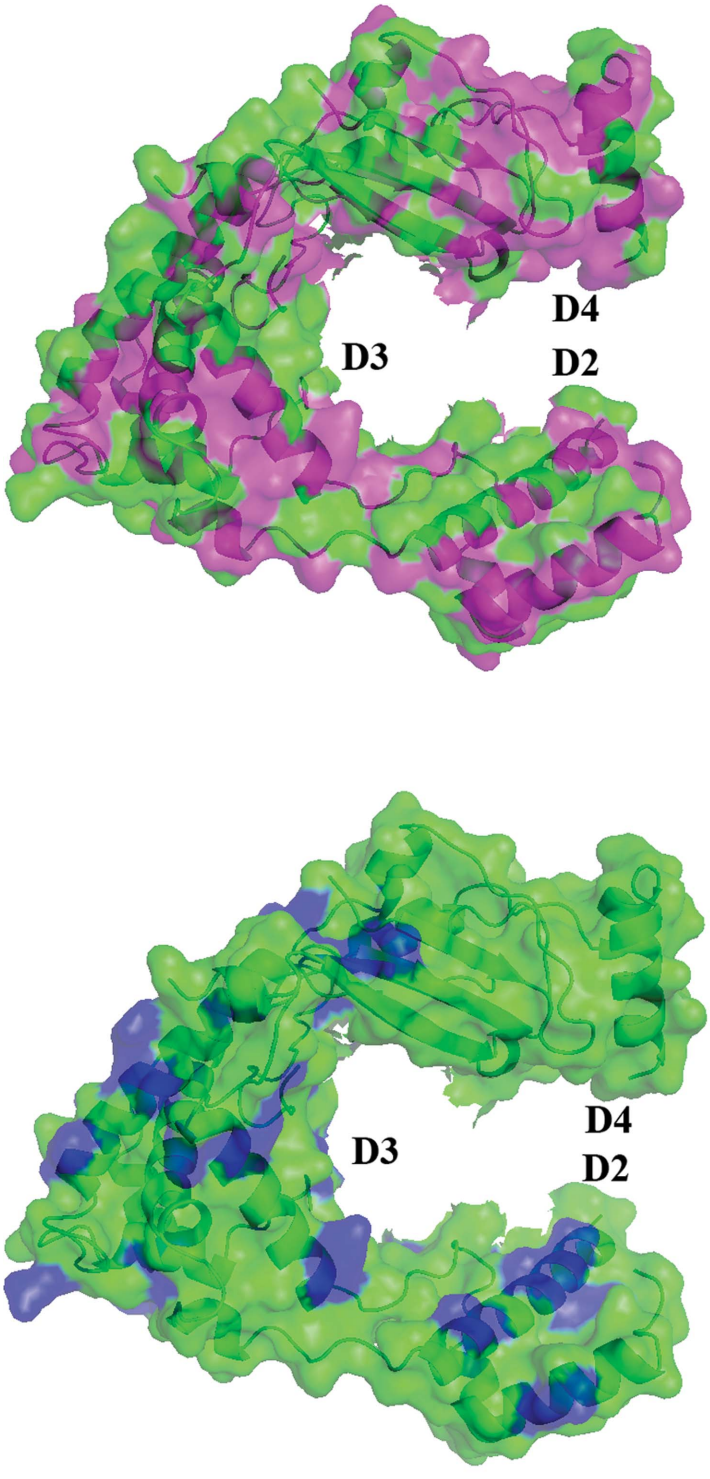

(*a*)

D2

NO.	PDB entry	PDB description	Z score	rmsd	%id
1	4e2l-D	FERRIC ENTEROBACTIN (ENTEROCHELIN) TRANSPORT	3.5	2.3	12
2	2jx4-A	VASOPRESSIN V2 RECEPTOR	3.5	2.4	10
3	3w5b-A	SERCA1A	3.5	2.4	5
4	3spa-A	RNA POLYMERASE, MITOCHONDRIAL	3.4	3.2	11
5	3b8o-C	LIPOPOLYSACCHARIDE BIOSYNTHESIS WZZE	3.4	2.5	5
6	3gnl-A	UNCHARACTERIZED PROTEIN, DUF633,	3.4	2.7	2
7	3nkz-B	FLAGELLAR PROTEIN FLIT	3.4	4.1	5
8	2uxw-A	VERY-LONG-CHAIN SPECIFIC ACYL-COA DEHYDROGENASE	3.4	2.4	4
9	3b8o-A	THERMOSTABLE LIPASE	3.3	2.5	5
10	3iza-A	APOPTOTIC FACTOR 1	3.3	3.3	7

D3

NO.	PDB entry	PDB description	Z score	rmsd	%id
1	4a56-A	PULLULANASE SECRETION PROTEIN PULS	4.8	3.4	11
2	4k0u-A	LIPOPROTEIN OUTS	4.6	3.5	9
3	3sol-A	TYPE II SECRETION PATHWAY RELATED PROTEIN	4.6	3.7	9
4	3uym-A	LIPOPROTEIN OUTS	4.5	3.5	9
5	3utk-B	LIPOPROTEIN OUTS	4.4	3.6	9
6	2xq2-A	SODIUM/GLUCOSE COTRANSPORTER	3.9	6.0	10
7	3m8a-I	NONSTRUCTURAL PROTEIN1	3.9	4.3	9
8	1nsl-B	NONSTRUCTURAL PROTEIN1	3.5	4.6	6
9	2zko-B	NONSTRUCTURAL PROTEIN1	3.5	4.7	8
10	1xeq-B	NONSTRUCTURAL PROTEIN1	3.4	5.7	6

D4

NO.	PDB entry	PDB description	Z score	rmsd	%id
1	1dkx-A	CHAPERONE PROTEIN DNAK	3.2	3.2	9
2	4jn4-B	CHAPERONE PROTEIN DNAK	2.6	3.4	10
3	2wjs-A	LAMININ SUBUNIT ALPHA-2	2.5	3.2	10
4	4jn4-A	CHAPERONE PROTEIN DNAK	2.5	3.4	10
5	3pve-B	AGRIN, AGRN PROTEIN	2.1	3.9	10

(*b*)

Figure 4
The characteristics of the membrane-anchoring module. (*a*) Distribution of hydrophobic residues (magenta, upper) and positive residues (blue, lower) on the surface (green). (*b*) Structural similarity searches of the three domains of the module performed by the *DALI* web server.

by the backbone N atoms of the conserved residues Gly71–Thr73 in the β2–α2 loop and Phe234–Ala238 in β4, α8 and the connecting loop (Supplementary Figs. S1 and S2*b*).

3.4. The inserted helices in the catalytic module

Further inspection revealed that prominent differences between the catalytic module and its homologues are the two inserted helices α1 (Ser22–Arg41) and α7 (Gly193–Ser218; Figs. 2*c* and 3*a*; Supplementary Fig. 2*a*). They are located on opposite sides of the catalytic domain and many of the residues are conserved (Supplementary Fig. S1). There are many basic residues in these helices, forming positively charged protuberances (such as the 195KKRR198 and 211KLRQR215 motifs in α7; Supplementary Fig. S2*c*). Moreover, several residues located in the middle of helix α7 are hydrophobic. Considering the relative location of these inserted helices, they may play a role in stabilizing the catalytic domain by holding it from both sides. The positive charge distribution combined with the hydrophobic characteristics enable these helices to interact with the negatively charged membrane or to assist the catalytic domain to adapt to the hydrophobic environment of the membrane.

3.5. Structural characteristics of the putative membrane-anchoring module

There are many hydrophobic residues distributed in the module, constituting a large continuous hydrophobic dominated surface and endowing the proteins with an overall amphipathic surface (Fig. 4*a*; Supplementary Fig. S1). For example, there are 34/52 hydrophobic residues in D2, which are distributed evenly in the helices (Supplementary Fig. S1). These residues form a hydrophobic dominated surface, which may adapt to the hydrophobic membrane conditions during their interaction. In addition, there are many basic residues distributed especially in D2 and D3 (Fig. 4*b*, Supplementary Fig. S1), such as the motif 515HKRRSR520 in α15 that forms a positively charged protuberance. These positive residues may be involved in recognizing the negative phospholipid head groups of the membrane for initial binding.

The *DALI* search revealed relatively lower structural similarities of the three domains that constitute the putative membrane-anchoring module to known structures (Fig. 4*b*). The closest homologue of D2 is the surface O-antigen lipopolysaccharide co-polymerase (PCP) from *Shigella flexneri* (PDB entry 4e2l), which is a periplasmic protein anchored in the inner membrane (Kalynych *et al.*, 2012). Structural superimpositions revealed that the long helices α15 and α16 in D2 have notable similarity to partial helices in the periplasmic domain of PCP (Supplementary Fig. S4*a*). Similarly, the best hits for D3 belong to periplasmic lipoproteins, suggesting that it is likely to be associated with periplasmic location. The long helices α13 and α19 in D3 superimpose well with helices α1 (H1) and α3 (H3) of the lipoproteins OutS, PulS and GspS (PDB entries 4a56, 4k0u and 3sol) from bacterial type II secretion systems (T2SS; Supplementary Fig. S4*b*), respectively. These lipoproteins target the corresponding integral outer membrane secretins through the periplasm to the outer membrane and allow functional T2SS to be assembled (Tosi *et al.*, 2011; Gu *et al.*, 2012; Rehman *et al.*, 2013). Interestingly, the *DALI* search revealed that the homologues of D4 only include molecular chaperones, such as DnaK and Hsp70s, and the glycoprotein laminin G-like (LG) domains. The sandwich conformation in this domain superimposes well with the polypeptide substrate-binding domain of *E. coli* DnaK (PDB entry 1dkx; Zhu *et al.*, 1996; Supplementary Fig. S4*c*) and the glycoprotein laminin G-like (LG) domains 1–3 (PDB entry 2wjs; Carafoli *et al.*, 2009).

Although many of the top homologues above belong to periplasmic or membrane proteins, the overall conformations of the three domains are novel and different from known structures. Their real role in periplasmic location or membrane interaction requires further investigation.

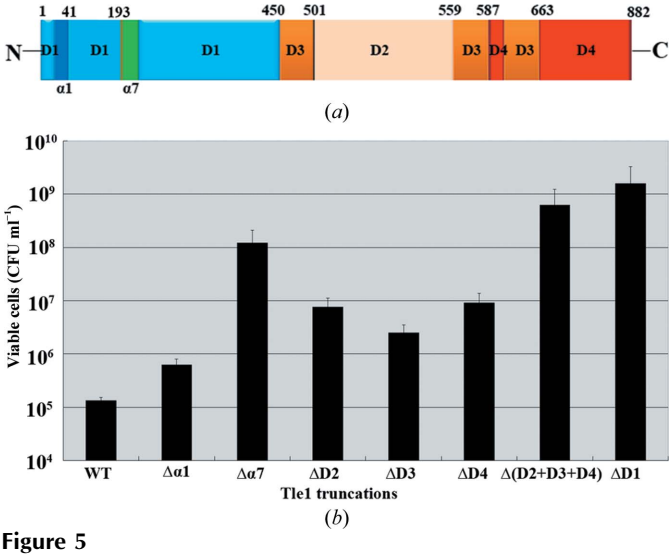

Figure 5
The roles of different domains/helices in defining Tle1 toxicity. (*a*) Truncation schematic of the domain organization of Tle1. (*b*) Effect of the expression of Tle1 truncations in the periplasm on *E. coli* growth.

3.6. The roles of different domains/helices in defining Tle1 toxicity

The roles of the three domains in the membrane-anchoring module and the inserted helices in the catalytic module in Tle1 antibacterial activity were further investigated by studying the effect of the expression of different truncations of Tle1 in the periplasm on *E. coli* growth (Figs. 5*a* and 5*b*). Surprisingly, compared with wild-type Tle1, deletion of helix α7 ($\Delta\alpha$7) significantly reduced the toxicity of Tle1, whereas deletion of helix α1 ($\Delta\alpha$1) had a negligible effect on its activity. Deletion of a single domain in the membrane-anchoring module (ΔD2, ΔD3 or ΔD4; Fig. 2*c*) only moderately reduced the toxicity of Tle1. However, when the whole module was deleted [Δ(D2+D3+ΔD4)] there was a complete loss of Tle1 toxicity; even the Western blot analysis showed that the expression of this truncation in the periplasm was significantly higher than that of the full-length protein (Supplementary Fig. S5*b*). This suggests the membrane-anchoring module is indispensable for

the antibacterial activity of the catalytic module in Tle1. Similarly, the expression of $\Delta\alpha7$ is also notably higher than that of the full-length protein (Supplementary Fig. S5*b*) and this indicated that its lower toxicity is largely not associated with increased protein expression.

3.7. Structural model of Tle1 targeting to the membrane

To investigate the interaction of Tle1 with the membrane, we carried out molecular-dynamics (MD) simulations on the extended open configuration of the putative membrane-anchoring module embedded into a bilayer mainly consisting of 1-palmitoyl-2-oleoyl-*sn*-glycero-3-phosphoethanolamine (POPE; Figs. 6*a* and 6*b*). The missing residues in several loops were added with *MODELLER*. For example, residues Trp663–Glu674 in the loop $\alpha20$–$\beta12$ in D3 neighbouring the active site were not observed in the present structure. This flexibility may be caused by the absence of the substrate and may be essential for substrate recognition and catalysis. The established model system was found to be stable over a 50 ns MD simulation at constant temperature and pressure.

In this model, consistent with the cell-toxicity assay results, not only the amphipathic helices $\alpha15$ and $\alpha16$ in D2 but also the amphipathic β-sandwich structure in D4, including $\beta10$, $\beta13$ and $\beta14$ with the two short helices $\alpha24$ and $\alpha25$, are embedded into the negatively charged membrane surface (Figs. 6*c* and 6*d*). Moreover, the inserted positively charged helix $\alpha7$ (especially the basic motif KKRR) and the adjacent $\alpha6$ in the catalytic module are also found to be close to the membrane, and the flexible loop $\alpha7$ and $\alpha9$ is embedded into the bilayer. More importantly, many residues in these regions that potentially interact with the bilayer are conserved or highly conserved (Supplementary Fig. S1). Meanwhile, D3 is not integrated into the bilayer but is rather located in the periplasmic space in this model. It is directly facing and proximal to the bilayer (Fig. 6*b*), which may establish direct

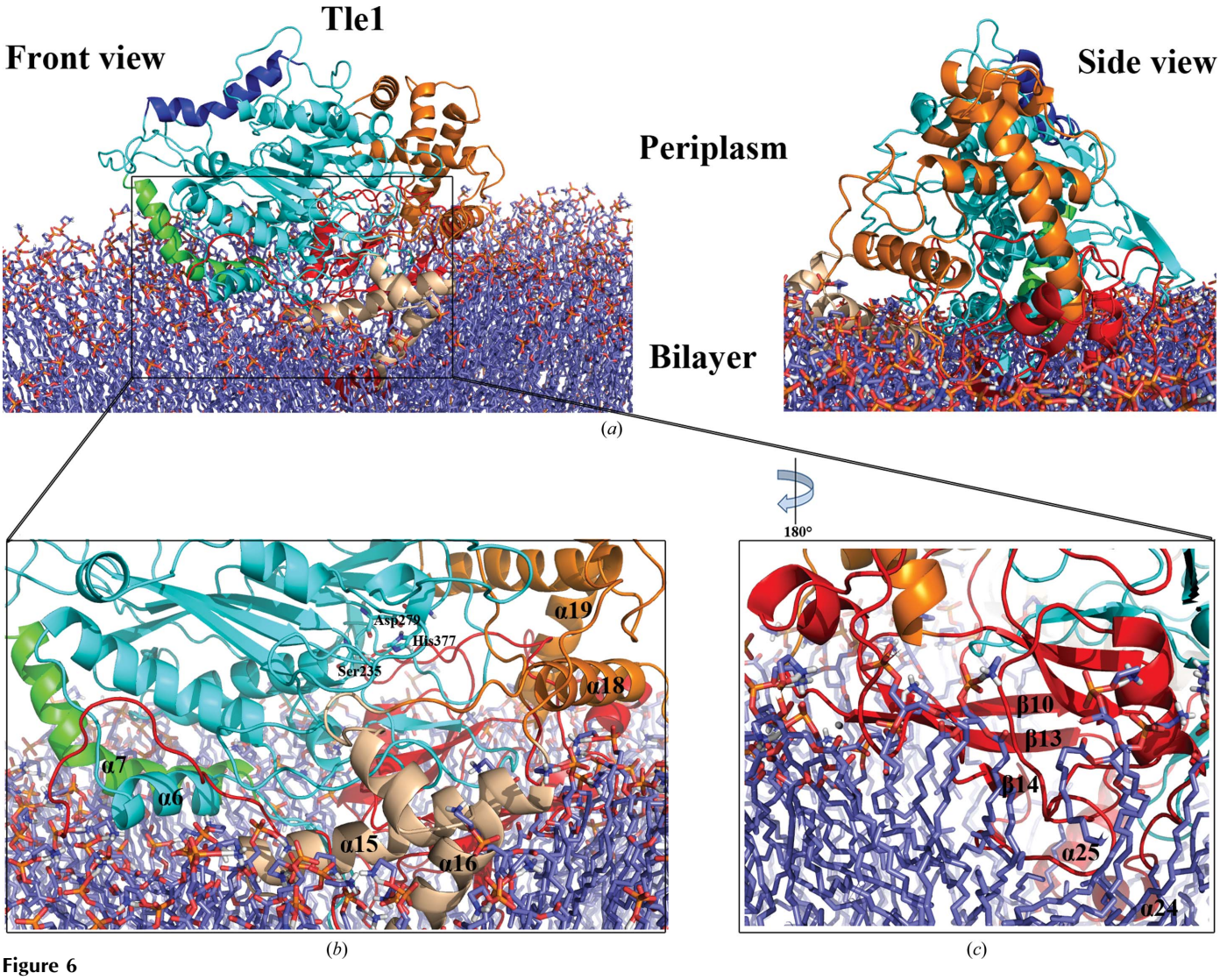

Figure 6
The putative membrane-targeting mechanism of Tle1. (*a*) The structure of Tle1 modelled into a POPE bilayer (purple sticks) by a molecular-dynamics simulation: front view and side view. The colours of the different parts of Tle1 are the same as in Fig. 1(*c*). (*b*, *c*) The helices and strands embedded into the bilayer or close to the interface are labelled. The catalytic triad residues are shown as cyan sticks.

access to extract the phospholipids to the catalytic triad in the catalytic pocket. Similar observations were also made for human cytosolic phospholipase A_2 ($cPLA_2$). The highly hydrophobic regions 35–39 and 96–98 in the N-terminal lipid-binding domain (C2 domain) can penetrate into the lipid phase, whereas the regions 268–279 and 466–470 in the catalytic domain can mediate $cPLA_2$ interfacial binding through electrostatic interactions with phospholipid head groups (Burke *et al.*, 2008; Dennis *et al.*, 2011).

4. Discussion

In some secreted lipase homologues of the catalytic module, there are inserted α/β subdomains that form a cap region or the lid domain sits on top of the α/β-hydrolase core. These inserted subdomains function as a lid that can open or close the active site for exposure to solvents and substrates or as a motif that shapes the active site for the accommodation of appropriate substrates (Lai *et al.*, 2011; Schalk-Hihi *et al.*, 2011; Chow *et al.*, 2012). However, there seems to be no such inserted lid-domain structure in the catalytic module of Tle1. Formation of the catalytic pocket in Tle1 requires helices $\alpha12$ and $\alpha20$ and the loop $\alpha20$–$\beta12$ in D3, which sits above the α/β-hydrolase core. More importantly, deletion of D3 can obviously reduce the toxicity of Tle1 owing to destruction of the catalytic pocket (Fig. 5*b*). Meanwhile, although D3 is not integrated into the bilayer, as observed in the MD simulations, this domain is directly facing the membrane. It may provide an accommodating environment or establish direct access to extract the phospholipids to the catalytic triad in the catalytic pocket (Figs. 6*b* and 6*c*). Therefore, D3 is likely to play a role similar to the functions of the inserted lid domains or the cap regions in not only providing a protective environment for the catalytic core but also being essential in defining selectivity in the hydrolysis of phospholipids by Tle1.

All of the recently identified T6SS lipase effectors have lipase domains and have been suggested to target membrane-associated lipids (Russell *et al.*, 2013; Dong, Ho *et al.*, 2013; Miyata *et al.*, 2011). VasX has been shown to localize to the bacterial membrane and can interact with membrane phospholipids *via* its pleckstrin-homology (PH) domain *in vitro* (Miyata *et al.*, 2011), but the membrane-targeting process remains uncharacterized. In this study, the MD simulation based on our Tle1 structure provides a reasonable model of the embedding of the membrane-anchoring module into the bilayer. Considering the important role of the basic helix $\alpha7$ in Tle1 toxicity (Fig. 6*a*), initial lipid recognition and binding may occur *via* positively charged residues mainly located in $\alpha7$, D2 and D3 (Fig. 3*b* and Supplementary Fig. S2*c*), followed by membrane insertion and transition to the open configuration of Tle1. Similarly, the human 'saposin fold' family of membrane-interacting or membrane-lytic sphingolipid activator proteins, such as saposin C and granulysin, rely on positively charged clusters on their surface to interact with negatively charged lipid head groups to trigger their liposomal vesicle fusion activities (Anderson *et al.*, 2003; Rossmann *et al.*, 2008).

From its strong hydrophobic character, structural similarity to some periplasmic or membrane proteins and important role in antibacterial activity, it is reasonable to postulate that the open conformation of the membrane-anchoring module may play a critical role in Tle1 targeting to the bacterial membrane. It may serve to position the protein close to the negatively charged membrane and embed it into or penetrate the phospholipid layer. Moreover, since the substrate phospholipids in the fluid bilayer are lined up in a two-dimensional interface, a single phospholipid molecule is required to dissociate from the bilayer. The phospholipid would then be extracted to the open funnel of the membrane-anchoring module and be inserted into the active site accompanied by certain conformational changes. Upon substrate binding, the putative membrane-anchoring module would close over the bound substrate, which is hydrolyzed by the catalytic module.

Another interesting question is how these T6SS lipase effectors, including the Tle family members TseL and VasX, diffuse through the T6SS injection needle. They have relatively large molecular weights (~60–120 kDa) and belong to the VgrG-associated proteins (Russell *et al.*, 2013; Dong, Ho *et al.*, 2013; Miyata *et al.*, 2011), and TseL has been found to directly interact with VgrG3 during its secretion (Dong, Ho *et al.*, 2013). Any of the three dimensions of Tle1 (Fig. 2*a*) is much larger than the internal diameter of the Hcp1 tube and the VgrG spike (35–40 Å), and therefore it would seem to be unable to be transported into the T6SS injection needle in the present conformation. A reasonable explanation is that they may be unfolded or partly unfolded into a polypeptide chain before injection into the Hcp needle or during transportation. After secretion into the periplasm of the recipient cell, they will be refolded into the functional state. Instead, the T6SS secreted effectors Tse1 and Tse2 are smaller proteins (<20 kDa; Chou *et al.*; Ding *et al.*, 2012) and make direct interaction with the hexameric Hcp ring to bind into its internal cavity (Silverman *et al.*, 2013). They may be directly injected into the recipient cell and transported in their functional state. Although there is an elongated fold in Tse3 (44 kDa), it can also be accommodated within the Hcp1 tube (Li *et al.*, 2013). Therefore, the dimensions of these T6SS effectors may be one of the factors that determine their different transportation mechanisms.

Our comprehensive studies on Tle1, including the novel crystal structure with an open conformation, biochemical characterization and molecular-dynamics simulations, suggest that it is a unique phospholipase targeting the bacterial membrane and represents the first member of the T6SS phospholipase effectors to be structurally described. These studies provide structural insight into the catalytic mechanism of Tle1 and contribute to a better understanding of the antibacterial activities of the T6SS phospholipase effector families.

We thank the staff of beamline station 3W1A at Beijing Synchrotron Radiation Facility (BSRF) for providing technical support and for many fruitful discussions. This study was financially supported by grants from the National Basic

Research Program of China (2012CB917203) and the National Natural Science Foundation of China (10979005 and 31200552). All of the authors have declared that no conflicts of interest exist.

References

Adams, P. D. *et al.* (2010). *Acta Cryst.* D**66**, 213–221.
Anderson, D. H., Sawaya, M. R., Cascio, D., Ernst, W., Modlin, R., Krensky, A. & Eisenberg, D. (2003). *J. Mol. Biol.* **325**, 355–365.
Berendsen, H. J. C., Postma, J. P. M. & van Gunsteren, W. F. (1984). *J. Chem. Phys.* **81**, 3684–3690.
Berger, O., Edholm, O. & Jähnig, F. (1997). *Biophys. J.* **72**, 2002–2013.
Burke, J. E., Hsu, Y.-H., Deems, R. A., Li, S., Woods, V. L. Jr & Dennis, E. A. (2008). *J. Biol. Chem.* **283**, 31227–31236.
Carafoli, F., Clout, N. J. & Hohenester, E. (2009). *J. Biol. Chem.* **284**, 22786–22792.
Chou, S., Bui, N. K., Russell, A. B., Lexa, K. W., Gardiner, T. E., LeRoux, M., Vollmer, W. & Mougous, J. D. (2012). *Cell Rep.* **1**, 656–664.
Chow, J. *et al.* (2012). *PLoS One*, **7**, e47665.
Cowtan, K. (2006). *Acta Cryst.* D**62**, 1002–1011.
Darden, T., York, D. & Pedersen, L. (1993). *J. Chem. Phys.* **98**, 10089.
DeLano, W. (2002). *PyMOL*. http://www.pymol.org.
Dennis, E. A., Cao, J., Hsu, Y.-H., Magrioti, V. & Kokotos, G. (2011). *Chem. Rev.* **111**, 6130–6185.
Ding, J., Wang, W., Feng, H., Zhang, Y. & Wang, D.-C. (2012). *J. Biol. Chem.* **287**, 26911–26920.
Dong, C., Zhang, H., Gao, Z.-Q., Wang, W.-J., She, Z., Liu, G.-F., Shen, Y.-Q., Su, X.-D. & Dong, Y.-H. (2013). *Biochem. J.* **454**, 59–68.
Dong, T. G., Ho, B. T., Yoder-Himes, D. R. & Mekalanos, J. J. (2013). *Proc. Natl Acad. Sci. USA*, **110**, 2623–2628.
Dundas, J., Ouyang, Z., Tseng, J., Binkowski, A., Turpaz, Y. & Liang, J. (2006). *Nucleic Acids Res.* **34**, W116–W118.
Emsley, P., Lohkamp, B., Scott, W. G. & Cowtan, K. (2010). *Acta Cryst.* D**66**, 486–501.
Eswar, N., Webb, B., Marti-Renom, M. A., Madhusudhan, M. S., Eramian, D., Shen, M.-Y., Pieper, U. & Sali, A. (2006). *Curr. Protoc. Bioinformatics*, Unit 5.6. doi:10.1002/0471250953.bi0506s15.
Gu, S., Kelly, G., Wang, X., Frenkiel, T., Shevchik, V. E. & Pickersgill, R. W. (2012). *J. Biol. Chem.* **287**, 9072–9080.
Hess, B., Bekker, H., Berendsen, H. J. C. & Fraaije, J. G. E. M. (1997). *J. Comput. Chem.* **18**, 1463–1472.
Hess, B., Kutzner, C., van der Spoel, D. & Lindahl, E. (2008). *J. Chem. Theory Comput.* **4**, 435–447.
Hood, R. D. *et al.* (2010). *Cell Host Microbe*, **7**, 25–37.
Jani, A. J. & Cotter, P. A. (2010). *Cell Host Microbe*, **8**, 2–6.
Kalynych, S., Yao, D., Magee, J. & Cygler, M. (2012). *J. Biol. Chem.* **287**, 15696–15705.
Krissinel, E. & Henrick, K. (2004). *Acta Cryst.* D**60**, 2256–2268.
Lai, K. K., Stogios, P. J., Vu, C., Xu, X., Cui, H., Molloy, S., Savchenko, A., Yakunin, A. & Gonzalez, C. F. (2011). *PLoS One*, **6**, e23269.
Li, L., Zhang, W., Liu, Q., Gao, Y., Gao, Y., Wang, Y., Wang, D. Z., Li, Z. & Wang, T. (2013). *J. Biol. Chem.* **288**, 30607–30613.
Miyata, S. T., Kitaoka, M., Brooks, T. M., McAuley, S. B. & Pukatzki, S. (2011). *Infect. Immun.* **79**, 2941–2949.
Montersino, S., Orru, R., Barendregt, A., Westphal, A. H., Van Duijn, E., Mattevi, A. & Van Berkel, W. J. H. (2013). *J. Biol. Chem.* **288**, 26235–26245.
Morris, G. M., Goodsell, D. S., Halliday, R. S., Huey, R., Hart, W. E., Belew, R. K. & Olson, A. J. (1998). *J. Comput. Chem.* **19**, 1639–1662.
Nosé, S. (1984). *Mol. Phys.* **52**, 255–268.
Oostenbrink, C., Villa, A., Mark, A. E. & van Gunsteren, W. F. (2004). *J. Comput. Chem.* **25**, 1656–1676.
Otwinowski, Z. & Minor, W. (1997). *Methods Enzymol.* **276**, 307–326.
Parrinello, M. & Rahman, A. (1981). *J. Appl. Phys.* **52**, 7182–7190.
Rehman, S., Gu, S., Shevchik, V. E. & Pickersgill, R. W. (2013). *Acta Cryst.* D**69**, 1381–1386.
Rossmann, M., Schultz-Heienbrok, R., Behlke, J., Remmel, N., Alings, C., Sandhoff, K., Saenger, W. & Maier, T. (2008). *Structure*, **16**, 809–817.
Russell, A. B., Hood, R. D., Bui, N. K., LeRoux, M., Vollmer, W. & Mougous, J. D. (2011). *Nature (London)*, **475**, 343–347.
Russell, A. B., LeRoux, M., Hathazi, K., Agnello, D. M., Ishikawa, T., Wiggins, P. A., Wai, S. N. & Mougous, J. D. (2013). *Nature (London)*, **496**, 508–512.
Schalk-Hihi, C. *et al.* (2011). *Protein Sci.* **20**, 670–683.
Schmidt, T. H. & Kandt, C. (2012). *J. Chem. Inf. Model.* **52**, 2657–2669.
Schwarz, S., Hood, R. D. & Mougous, J. D. (2010). *Trends Microbiol.* **18**, 531–537.
Sheldrick, G. M. (2010). *Acta Cryst.* D**66**, 479–485.
Silverman, J. M., Agnello, D. M., Zheng, H., Andrews, B. T., Li, M., Catalano, C. E., Gonen, T. & Mougous, J. D. (2013). *Mol. Cell*, **51**, 584–593.
Terwilliger, T. C. (2000). *Acta Cryst.* D**56**, 965–972.
Tosi, T., Nickerson, N. N., Mollica, L., Jensen, M. R., Blackledge, M., Baron, B., England, P., Pugsley, A. P. & Dessen, A. (2011). *Mol. Microbiol.* **82**, 1422–1432.
Wei, Y., Gao, Z.-Q., Otsuka, Y., Naka, K., Yonesaki, T., Zhang, H. & Dong, Y.-H. (2013). *Mol. Microbiol.* **90**, 956–965.
Zhang, H., Zhang, H., Gao, Z.-Q., Wang, W.-J., Liu, G.-F., Xu, J.-H., Su, X.-D. & Dong, Y.-H. (2013). *J. Biol. Chem.* **288**, 5928–5939.
Zhu, X., Zhao, X., Burkholder, W. F., Gragerov, A., Ogata, C. M., Gottesman, M. E. & Hendrickson, W. A. (1996). *Science*, **272**, 1606–1614.